Numerical Simulation of Heat Transfer and Nanoparticle Transport in a Nanofluid within a Tumour Surrounding a Blood Vessel

A.M. Ismaeel[1,2,*], R.S Kamel[1,3], M.R. Hedar[4], F.M. Hady[1]
[1]*Department of Mathematics, Faculty of Science, Assiut University, Assiut, Egypt*
[2]*Faculty of Basic Sciences, King Salman International University, South Sinai, Egypt*
[3] *Higher Institute of Engineering and Technology, Minya, Egypt*
[4]*Department of Mathematics, Faculty of Science, Minia University, Minya, Egypt*
**Corresponding author: a.ismaeel@aun.edu.eg*

Abstract

A Newtonian nanofluid containing suspended nanoparticles can substantially improve heat transfer due to enhanced energy transport mechanisms. This theoretical study investigates heat and mass transfer in biological tissues using such a nanofluid under a magnetic field. These properties have promising medical and engineering applications. The nonlinear governing equations were transformed into ordinary differential equations using similarity variables and numerically solved with MATLAB boundary value problem solver bvp4c, subject to appropriate boundary conditions. Results demonstrated increasing the heat source parameter dramatically raised tumor interstitial temperature. This heating, along with improved nanoparticle accumulation within the tumor due to the thermal effects, are together essential for effective hyperthermia treatment. The model provides new insights into tuning heat and mass transport mechanisms in biological tissues via nanofluids for therapeutic applications. Therefore, the findings of this study may improve the efficacy of thermal therapy in treating cancer.

Keywords : Nanofluids, Brownian motion, Newtonian fluid, biological tissues, cancer treatment.

Article Highlights

1- This work examined magnetic field effects on heat transfer and nanoparticle (NP) transport in a Newtonian nanofluid within tissue surrounding a blood vessel.
2- Elevating the external heat source power distributes NPs and increases tumour temperature.
3- Boosting the thermophoresis coefficient enhances NP dispersion into tissue.
4- Tuning heat and mass transport mechanisms via nanofluids shows promise for advancing hyperthermia cancer treatment.

1- Introduction

Nanotechnology has generated substantial curiosity and attention from researchers as a leading scientific area examining nanofluids because of nanofluids significance in biological and medical uses [1]. Nanofluids significantly contribute to many technological devices due to their superior thermal conductivity compared to other liquids. Choi [2] conducted some of the first nanotechnology experiments, introducing minuscule metal particles into base fluids. He studied their physical and thermal properties and discovered nanoparticles (NPs) possess superior thermal characteristics versus other fluids. Lee et al. [3] examined the thermal and physical properties of oxide nanofluids. Their results revealed these liquids with a small nanoparticle concentration have much better heat transfer properties than liquids without nanoparticles. Choi et al. [4] put forth theoretical concepts explaining the abnormal thermal performance of nanotube suspensions. Nanotubes display the strongest thermal conductivity enhancement among nanostructured materials dispersed in liquids, opening avenues for diverse nanotube uses. Kang et al. [5] investigated the thermal characteristics of highly dispersed diamond, silver and silica NPs. Wang et al. [6] analysed convection heat transfer using solid NPs in base fluids. Their findings showed NPs significantly boost thermal conductivity and heat transfer. Buongiorno [7] explored the physical and thermal characteristics of nanofluids. Compared to their base fluids, nanofluids possess improved thermal conductivity and single-phase heat transfer coefficients. Notably, standard pure-fluid correlations like Dittus-Boelter's cannot elucidate the rises in heat transfer coefficients beyond basic thermal conductivity influences. Ghalambaz et al. [8] studied the characteristics and impacts of Brownian motion and thermal conductivity on hybrid nanofluid flow. Results demonstrated intensified heat transfer by adding hybrid NPs for conduction-dominant, low Rayleigh number regimes. Rasool et al. [9] examined magnetohydrodynamic (MHD) Williamson nanofluid flow through porous media over a flat surface. Outcomes showed nanofluid motion substantially intensified Brownian motion and heat transfer. Skin friction, Nusselt number and Sherwood number aligned with past Williamson nanofluid studies. Menni et al. [10] used computational fluid dynamics (CFD) to conduct hydrodynamic and thermal analyses of forced water convection, examining turbulent flow and forced-convection in obstructed channels like those found in heat exchangers and solar collectors. This study revealed compelling results advancing professional knowledge. Bhattacharyya et al. [11] examined the physical and thermal properties of carbon nanotubes, as well as liquid velocity, skin friction coefficient and temperature behaviour. A major finding was that single-walled carbon nanotube (SWCNT) nanofluids generate less drag and better heat transfer than multi-walled (MWCNT) nanofluids. Malik et al. [12] studied the physical and thermal characteristics of Sisko fluid flow through a cylinder. Results demonstrated the Sisko fluid coefficient and fluid velocity substantially rose, while velocity was hampered as the magnetic field intensity escalated.

Recently, researchers have invested great interest in nanofluid dynamics due to their utility in biomedical applications like drug delivery and protein detection. Patel et al. [13] reviewed nanotechnology uses in drug delivery systems and cancer therapies. Localized, targeted drug transport via NPs and nanoshells show particular promise as emerging nanomedicines and nanodevices for cancer treatment, including quantum dots, nanowires, carbon nanotubes, nanocantilevers and nanopores. McCarroll et al. [14] focused their review on leveraging nanotechnology for pancreatic cancer diagnosis, imaging, and therapeutic agent delivery. Purushotham et al. [15] synthesized and evaluated drug-loaded polymer-coated magnetic NPs (MNPs) as multimodal cancer therapy agents. Results demonstrated excellent hyperthermia induction and drug release capabilities for these doxorubicin-loaded MNPs when exposed to an alternating magnetic field. This reveals their potential for combined targeting, hyperthermia and controlled drug release cancer treatments. Abbasi et al. [16] examined silver-water nanofluid transport properties under a magnetic field. Findings showed nanofluid maximum velocity declined as the velocity slip coefficient rose, while temperature increased. Kothandapani et al. [17] studied peristaltic nanofluid transport characteristics in a magnetic field. Outcomes revealed escalating shear pressure with rising Hartmann number. Hayat et al. [18] employed a 3D model of hybrid nanofluids to boost heat transfer beyond conventional fluids. Hayat et al. [19] visualized and compared water and hybrid nanofluids, finding hybrid fluid heat transfer was much higher. Nadeem et al. [20] explored hybrid nanofluid transport in a magnetic field within a cylinder. The hybrid nanofluid thermal conductivity and heat transfer exceeded regular liquids. Nadeem et al. [21] analyzed hybrid nanofluids using nanosized surface particles to improve heat transfer versus nanopolar fluids. Finally, Mansour et al. [22] developed a 2D model of nanoparticle-blood transport in a tumour-surrounded vessel. Results showed blood temperature inside the vessel increased and NP concentration around the tumour decreased with greater NP extravasation. Bali et al. [23] presented a study and explained how intratumor delivery of nanoparticles causes diffusion across blood capillary walls into neighboring tissues. This causes the walls of the sick capillaries to open up and allow nanoparticles to enter the tumor tissue. The findings showed that compared to other shapes, brick-shaped nanoparticles diffuse more quickly. Bali et al. [24] Offered many mathematical models for the use of nanotechnology in the treatment of cardiovascular disorders. Additionally, learn about mathematical modeling to comprehend the nature, size, and form of nanoparticles. Hewlin et al. [25] Simulated implant assisted medical drug targeting (IA-MDT) using induced magnetism to deliver patient-specific therapeutic agent dosages to targeted cardiovascular system areas was examined computationally. and that is accomplished by implanting a stent that is only slightly magnetizable at a diseased carotid artery site. The findings demonstrated that the particle density reduced along the axial direction, particularly after the stented region, as evidenced by the trapped particles on the

vessel wall along the axial flow direction. Hewlin et al. [26] Described the computational results and methods of simulated medical drug targeting (MDT) using induced magnetism, which is meant to be used in a Circle of Willis (CoW) model to deliver intravenous therapeutic agent doses that are customized to each patient. Particle capture efficiency was observed to improve with increasing magnetic field strengths, larger particle diameter sizes (1 μm and above), and slower blood flow velocity. Stanley et al. [27] Presented a novel method for employing a standard 3-D inkjet printing process to create optically clear stiff 3-D printed anatomical artery models that are appropriate for PIV analysis. The outcomes of this study indicate great potential for using the proposed methodology to the creation of 3-D printed anatomical models for PIV experiments.

The literature has not extensively explored the application of nanofluid flow within biological tissues. This study looks into the topic of heat transmission and NP mass transit within the interstitial fluid, which is the fluid that fills the gaps between cells in the tissue in the extracellular matrix. As a result, a horizontal cylinder was used to depict the blood vessel segment, as seen in **Fig. 1**. The NPs were considered to have been injected into a blood artery and then extravasated into the surrounding tissue. This is accomplished by exposing the tissues around the blood vessels to an external heat source (alternating magnetic field). In order to approach the problem in three dimensions, it is assumed that the cancer is homogenous in the circumference direction, taking into account the accumulation of NPs within the tumour and its temperature. This work uses an external alternating magnetic field to heat NPs in a manner similar to thermal treatment for treating tumors.

The manuscript is organized as follows: The magnetohydrodynamic nanofluids, their inherent thermal properties, and their applications in biomedicine are all introduced in the **introduction**. Both the mathematical model and the formulation of the problem are presented in **Section 2**. The numerical solution method is described in the next part (**Section 3)**., **Section 4** presents the findings and an explanation of the mathematical model, and **Section 5** presents the manuscript's conclusion.

2- Formulation of the problem

A mathematical model was developed to analyse heat transfer in a Newtonian nanofluid flowing around a horizontal cylinder with an alternating magnetic field with strength B_0 acts in the axial direction, which heats up the tissue surrounding the vessel as depicted in **Fig. 1**. The governing equations were formulated in cylindrical coordinates, where r represents the radial direction and z denotes the axial direction along the cylinder length (**Fig. 1**). T and C indicate the nanofluid temperature and NP concentration within the blood vessel, respectively. An

external heat source warms the tissue adjacent to the vessel. To simplify the model, the problem was restricted to two dimensions, considering the tumour third dimension as homogeneous. Consequently, the following equations were derived to simulate nanoparticle transport in the tumour [28]:

$$\frac{\partial(ru)}{\partial r} + r\frac{\partial w}{\partial z} = 0 \tag{1}$$

$$\left(u\frac{\partial u}{\partial r} + w\frac{\partial u}{\partial z}\right) = \frac{-1}{\rho}\frac{\partial p}{\partial r} + \nu\left(\frac{\partial^2 u}{\partial r^2} + \frac{1}{r}\frac{\partial u}{\partial r} - \frac{u}{r^2}\right) \tag{2}$$

$$\left(w\frac{\partial w}{\partial z} + u\frac{\partial w}{\partial r}\right) = \frac{-1}{\rho}\frac{\partial p}{\partial z} + \nu\left(\frac{\partial^2 w}{\partial r^2} + \frac{1}{r}\frac{\partial w}{\partial r}\right) - \frac{\sigma_0 B_0^2}{\rho}\, w \tag{3}$$

$$w\frac{\partial T}{\partial z} + u\frac{\partial T}{\partial r} = \alpha\left(\frac{\partial^2 T}{\partial r^2} + \frac{1}{r}\frac{\partial T}{\partial r}\right) + \tau\left(\frac{D_B}{\rho_p}\left(\frac{\partial T}{\partial r}\frac{\partial C}{\partial r}\right) + \frac{D_T}{T_\infty}\left(\frac{\partial T}{\partial r}\right)^2\right) + \frac{SAR}{\rho c_p}(C - C_\infty) \tag{4}$$

$$\left(w\frac{\partial C}{\partial z} + u\frac{\partial C}{\partial r}\right) = D_B\left(\frac{\partial^2 C}{\partial r^2} + \frac{1}{r}\frac{\partial C}{\partial r}\right) + \frac{D_T}{T_\infty}\left(\frac{\partial^2 T}{\partial r^2} + \frac{1}{r}\frac{\partial T}{\partial r}\right) \tag{5}$$

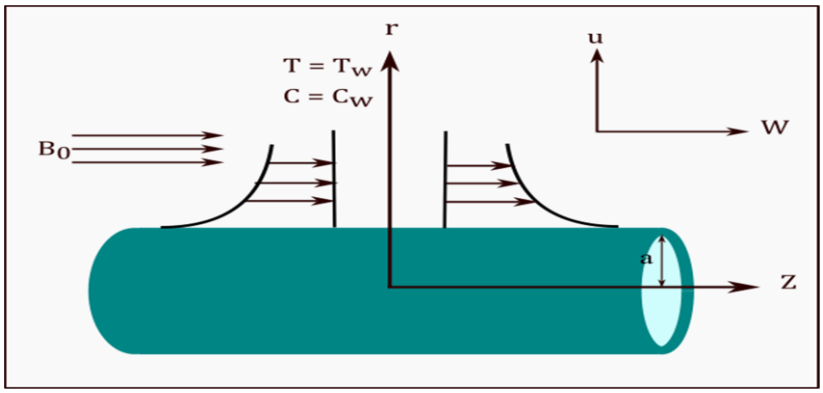

Figure 1. Geometry of the problem

where u and w are the fluid velocity components along the radial and axial directions, and C denotes the nanoparticle (NP) concentration. The parameters α, $p, \nu, \rho, \sigma, \sigma^*, D_B, D_T$ represent thermal diffusivity, pressure, dynamic viscosity, density, electrical conductivity, Stefan-Boltzmann constant, Brownian diffusion coefficient, and thermophoresis coefficient, respectively. Moreover, *SAR* (specific absorption rate) indicates the power or rate of non-ionizing radiation energy absorbed per unit mass of biological tissue. The model boundary conditions at the cylinder surface are:

$$\begin{aligned} r = a:&\quad u = U, \qquad w = 0, \qquad T = T_w, \qquad C = C_w \\ r \to \infty:&\quad \frac{1}{r}\frac{\partial}{\partial r}(ru) \to 0, \qquad uT - \alpha_{eff}\frac{\partial T}{\partial r} \to Q_H, \\ &\quad uC - D_B\frac{\partial C}{\partial r} - \frac{D_T}{T_\infty}\frac{\partial T}{\partial r} \to k \end{aligned} \tag{6}$$

The magnetic field effectively contributes to the process of heating the tumour tissue. Heat flux through the blood vessel wall into the blood vessel is defined as:

$$Q_H|_{r=a} = \left(uT - \alpha_{eff}\ \frac{\partial T}{\partial r}\right)_{r=a}. \tag{7}$$

The group of PDEs (1-6) can be simplified into a group of ODEs by applying the subsequent similarity transformations:

$$\eta = \left(\frac{r}{a}\right)^2,\ u = -Aa\left[\frac{f(\eta)}{\sqrt{\eta}}\right],\ w = 2Azf'(\eta),\ \theta(\eta) = \frac{T-T_\infty}{T_w-T_\infty},\ \phi(\eta) = \frac{C-C_\infty}{C_w-C_\infty}. \tag{8}$$

To eliminate pressure, Eq. (8) can be substituted into Eqs. (2) and (3), yielding:

$$-A^2a^2\rho\frac{ff'}{\eta} + A^2a^2\rho\frac{f^2}{2\eta^2} - 2A\nu\rho f'' = \frac{\partial p}{\partial \eta} \tag{9}$$

$$4\rho A^2 z\left(ff'' - f'^2\right) + \nu\rho\frac{8A}{a^2}z(f'' + \eta f''') - 2\sigma_0 B_0^2 Azf' = \frac{\partial p}{\partial z} \tag{10}$$

Integrating Eqs. (9) and (10) by parts allows the pressure to be expressed as:

$$p = p_0 - \rho\left(A^2a^2\frac{f^2}{2\eta} + 2\nu Af'\right) \Rightarrow \frac{\partial p}{\partial z} = 0 \tag{11}$$

After eliminating pressure, the following system of ODEs is obtained:

$$\eta f''' + f'' + R_e\ (ff'' - f'^2 - M_0\ f') = 0, \tag{12}$$

$$\eta\theta'' + (1 + R_e e\ P_r\ f)\,\theta' + \eta\left(N_b\phi'\theta' + N_t\theta'^2\right) + \lambda\ R_e\ P_r\ \frac{N_b}{N_t}\phi = 0, \tag{13}$$

$$\eta\phi'' + (1 + R_e\ S_c\ f)\,\phi' + \frac{N_t}{N_b}(\eta\theta'' + \theta') = 0, \tag{14}$$

where $M_0 = \frac{\sigma_0 B_0^2}{2\rho A}$ is the magnetic field parameter, $R_e = \frac{Aa^2}{2\nu}$ represents the Reynolds number, $P_r = \frac{\nu}{\alpha}$ denotes the Prandtl number and $S_c = \nu D_B^{-1}$ indicates the Schmidt number. Additionally, $N_b = \frac{\tau D_B(C_b - C_\infty)}{\nu\ C_\infty}$ stands for the Brownian motion parameter, $N_t = \frac{\tau D_T(T_b - T_\infty)}{\nu\ T_\infty C_\infty}$ symbolizes the thermophoresis parameter, and $\lambda = \frac{D_T\ SAR}{D_B\ T_\infty\ \rho c_p}$ indicates the heat source coefficient.

The corresponding boundary conditions are

$$\begin{aligned} &\eta = 1: f = -\gamma, f' = 0, \theta = 1, \qquad \phi = 1, \\ &\eta \to \infty: f' \to 0, -\eta_\infty^{-0.5} f(\theta + \xi_1) - B_2\eta_\infty^{0.5}\theta' \to Q_H^*, \\ &f(\phi + \xi_2) + B_1\eta_\infty\left(\phi' + \frac{N_t}{N_b}\theta'\right) = -\eta_\infty{}^{1/2}K, \end{aligned} \tag{15}$$

The heat flow rate per unit area at the wall of the vessel expressed in a dimensionless form is:

$$Q_H^*|_{\eta=1} = \gamma(1 + \xi_1) - B_2\ \theta' \tag{16}$$

where $B_1 = \frac{2D_B}{Aa^2} = \frac{1}{R_e\ S_c}$, $K = \frac{k}{ca(C_b - C_\infty)}$, $B_2 = \frac{2\alpha_{eff}}{Aa^2} = \frac{1}{R_e\ P_r}$,

$Q_H^* = \frac{Q_H}{Aa(T_b - T_\infty)}$, $\xi_1 = \frac{T_\infty}{T_b - T_\infty}$ and $\xi_2 = \frac{C_\infty}{C_b - C_\infty}$.

The local skin friction coefficient and local Nusselt number are respectively:

$$C_f = \frac{\tau_w}{\rho_f\, w^2/2} \quad , \quad \tau_w = \frac{4\, cz\mu_{nf}}{a}\, f''(1) \tag{17}$$

$$Nu_z = \frac{-aq_w}{\Delta T} \quad , \quad q_w = \frac{2(T_b - T_\infty)}{a}\, \theta'(1) \tag{18}$$

Substituting the dimensionless variables from Eq. (8) into Eqs. (17) and (18) gives:

$$C_f = f''(1) \tag{19}$$

$$Nu_z = -2\theta'(1) \tag{20}$$

The baseline parameter values used in this study are listed in **Table 1**.

Table 1: The parameter values list used in the mathematical model [28].

parameter	Value	parameter	value
K	*0.1*	R_e	*0.001*
Q_H^*	*0.1*	M_0	*0.1*
λ	*0.1*	N_t	*0.01*
ξ_1	*-1*	N_b	*0.5*
ξ_2	*1*	P_r	*7.56*
γ	*0.5*	S_c	*5*

Table 2: Comparisons showing the values of skin-friction coefficient and local Nusselt number for different values of R_e , P_r and N_b at $N_t = 0.2 = N_b = 0.1$, $S_c = 0.5$, $M_0 = 0$, $\lambda = 0$.

R_e	N_b	P_r	$f''(1)$ [31]	$-\theta'(1)$ [31]	$f''(1)$ Present study	$-\theta'(1)$ Present study
0.6			1.201788	0.8027277	1.201730	0.8027277
0.7			1.279712	0.7929646	1.279694	0.7929646
0.8			1.352200	0.7860852	1.352119	0.7860852
0.9			1.420093	0.7820039	1.420035	0.7820039
1.0			1.484220	0.7782725	1.484189	0.7782725
	0.3		1.116887	0.982304	1.116735	0.9827844
	0.4		1.116887	0.966789	1.116735	0.9641268
	0.5		1.116887	0.951512	1.116731	0.9457933
	0.6		1.116887	0.936472	1.116730	0.9277778
	0.7		1.116887	0.921667	1.116730	0.9100811
		0.6	1.116788	0.9138116	1.116732	0.9101446
		0.7	1.116887	0.9177397	1.116732	0.9174370
		0.8	1.116887	0.9216679	1.116732	0.9246256
		0.9	1.116887	0.9255941	1.116733	0.9217085
		1.0	1.116887	0.9295161	1.116733	0.9286845

3- Numerical Solution Method

The system of ODEs (12-15) can be reduced to a set of first-order ODEs. This ODE system can be numerically integrated using MATLAB [29]. Defining the following variables:

$$s_1 = f\ , s_2 = f', s_3 = f''\ ,\ \ s_4 = \theta,\ \ s_5 = \theta'\ , s_6 = \varphi, s_7 = \varphi'$$

Allows equations (12-16) to be expressed as:

$$\begin{aligned}
&s_1' = s_2, s_2' = s_3, s_4' = s_5, s_6' = s_7\\
&s_3' = f''' = \frac{-1}{\eta}\ [s_3 + R_e\ (s_1 s_3 - {s_2}^2\ -\ M_0\ \ s_2)],\\
&s_5' = \frac{-1}{\eta}\ [(1 + R_e\ P_r\ s_1\ )s_5 + \eta(N_b s_7 s_5 + N_t {s_5}^2) + \lambda\ R_e\ P_r\ \left(\frac{N_b}{N_t}\right) s_6\ ],\\
&s_7' = \frac{-1}{\eta}\ [(1 + R_e\ S_c\ s_1)s_7 + \frac{N_t}{N_b}(\eta s_5' + s_5)],
\end{aligned} \tag{21}$$

The boundary conditions (15) can be expressed in the form:

$$\begin{aligned}
&\eta = 1: \qquad s_1 = -\gamma,\quad s_2 = 0,\quad s_4 = 1,\qquad s_6 = 1,\\
&\eta \to \infty: \qquad s_2 = 0,\ \ -\eta_\infty^{-0.5}\ s_1(s_4 + \xi_1) - B_2\ \eta_\infty^{0.5} s_5 \to Q_H^*,\\
&s_1(\ s_6 + \xi_2) + B_1 \eta_\infty \left(\ s_7 + \frac{N_t}{N_b}\ s_5\right) = -{\eta_\infty}^{\frac{1}{2}} K,
\end{aligned} \tag{22}$$

The MATLAB boundary value problem solver bvp4c was utilized to solve the ODE system (21) and (22) with a relative error tolerance 10^{-5}, sufficient for solution accuracy [30]. An initial guess of $s_1 = s_2 = s_3 = s_4 = s_5 = s_6 = s_7 = 0$ is chosen to feed the boundary value problem solver. The results have been validated against the published data in the literature [31].

4- Results and Discussion

In this work, heat transport of a Newtonian nanofluid under a magnetic field flowing around a horizontal cylinder (representing a blood vessel) was examined. The system of equations (21) and (22) derived previously were solved numerically, utilizing 250 spatial grid points with a relative error tolerance of $O(10^{-5})$. Numerical results are graphically presented in **Figs.** 2 & 3.

We conducted an in-depth investigation into the effects of varying key parameter values on the interstitial fluid velocity, nanofluid temperature, and NP concentration distribution in tissue surrounding the blood vessel. As illustrated in **Fig.** 2(A), the interstitial fluid velocity increases near the vessel wall which improves the heat transfer in the interstitium through the blood stream. However, varying the NP extravasation velocity at the vessel wall, it significantly impacted NP accumulation and penetration depth into tumour tissue (**Fig.** 2(B)). This finding highlights the importance of NP extravasation dynamics from the blood vessel within targeting tumours.

Additional studies analysed how changes in thermophoresis and NP Brownian motion influence nanofluid heat transport. Thermophoresis coefficients

influenced nanofluid temperature, with escalating values producing noticeable temperature reductions (**Fig.** 2(C)). This relationship reveals opportunities for regulating heat delivery by tuning thermophoretic NP motion. Alternatively, intensifying NP Brownian motion uniformly raised interstitial fluid temperatures across the tumour (**Fig.** 2(D)), enabling potential hyperthermia approaches. Moreover, the Nusselt number quantifying convective heat exchange between the vessel and tissue strongly depended on the thermophoresis coefficient (**Fig.** 2(E)). Augmenting thermophoresis lowered the Nusselt number, signifying diminished heat transfer to tumour tissue.

Complementary simulations elucidated how parameters related to NP transport and heat generation impact temperature and NP distributions. **Figs.** 3(A)-(B) show escalating thermal diffusion coefficients substantially curbed NP concentration in the nanofluid, while higher mass diffusion coefficients enhanced accumulation. These trends manifest the complex interplay between thermally-driven and concentration-gradient NP transport. Additionally, raising Reynolds numbers simultaneously elevated interstitial fluid temperatures and reduced NP levels (**Figs.** 3(C)-(D)). The inverse correlation between heat transfer and NP accumulation implied by varying Reynolds numbers highlights the need to determine the optimal Reynolds number that balances sufficient thermal delivery to the tumour with adequate NP targeting. Finally, simulations applying an alternating magnetic field to induce heat generation revealed significantly heightened temperatures without external heat source intervention (**Fig.** 3(E)), indicating potential for tumour ablation. Moreover, magnetic field exposure enhanced NP localization in the tumour interior (**Fig.** 3(F)). Therefore, modulated magnetic field strengths can concurrently improve intra-tumour hyperthermia and NP targeting, which are prerequisites for successful thermotherapy.

In summary, our theoretical model provides a flexible platform for gaining mechanistic insights into the impact of tuneable parameters on nanofluid heat transport and NP fate in tumours. This knowledge lays the groundwork for identifying and implementing optimized operating conditions to maximize heat-mediated drug delivery and anti-tumour efficacy. Future efforts will focus on integrating additional complexities of the tumour microenvironment into the model, including heterogeneous vasculature, dynamic interstitial flows, and heat dissipation pathways. Extending the current model with these biological features represents an exciting direction for ultimately designing NP systems that synergistically leverage heat, drug transport, and vascular access to treat tumours.

5- Conclusion

This work examined heat transfer and NP transport in a Newtonian nanofluid flowing around a blood vessel within tumour tissue under a magnetic field. The

impacts of the velocity of interstitial fluid, heat absorption by tissue, thermal radiation, and heat conduction were examined and analysed. Key findings are summarized:

- Elevating extravasation velocity of interstitial fluid from the blood vessel into tissue enhances cooling, reducing external heat source impacts.
- Increasing the mass flux coefficient K causes semi-homogeneous NP accumulation in the tumour, limiting transport by Brownian motion.
- NP delivery can be improved by raising the thermophoresis coefficient.
- Boosting the external heat source power λ distributes NPs and increases tumour temperature.

This study incorporates certain simplifying assumptions that warrant further exploration in subsequent research. For example, the current model treats the tissue as a homogeneous porous medium, an approximation that does not hold true for tumours [32]. Furthermore, the model presumes a constant fluid flux across the vessel wall, a parameter that ought to be dictated by the blood flow within the blood vessel. Future work should aim to refine these aspects for a more accurate representation.

In summary, precise regulation of parameters influencing interstitial flow, heat transfer, and NP transport could enable optimized hyperthermia treatments. Further work is warranted exploring system dynamics.

Conflict of Interest Statement

The authors affirm that they have no known financial or interpersonal conflicts that would have appeared to have an impact on the research presented in this publication.

Data Availability

Not applicable.

Funding

Not applicable.

Reference

[1] Bayda, S., Adeel, M., Tuccinardi, T., Cordani, T., & Rizzolio, F. (2020). The history of nanoscience and nanotechnology: From chemical-physical applications to nanomedicine. *Molecules*, 25(1), 1-15. https://doi.org/10.3390/molecules25010112

[2] Choi, S. U. S. (1995). Enhancing Thermal Conductivity of Fluids with Nanoparticles. In The Proceedings of the 1995 ASME Int. Mech. Engg. Congress and Exposition (pp. 99-105). San Francisco USA: ASME.

[3] Lee, S., Choi, S. U. S., Li, S., & Eastman, J. A. (1999). Measuring Thermal Conductivity of Fluids Containing Oxide Nanoparticles. *ASME Journal of Heat Transfer*, 121, 280-289. https://doi.org/10.1115/1.2825978

[4] Choi, S. U. S., Zhang, Z. G., Yu, W., Lockwood, F. E., & Grulke, E. A. (2001). Anomalous Thermal Conductivity Enhancement in Nanotube Suspensions. *Applied Physics Letters*, 79(14), 2252-2254. https://doi.org/10.1063/1.1408272

[5] Kang, H. U., Kim, S. H., & Oh, J. M. (2006). Estimation of Thermal Conductivity of Nanofluid Using Experimental Effective Particle Volume. *Experimental Heat Transfer*, 19(3), 181-191. https://doi.org/10.1080/08916150600619281

[6] Wang, X., & Mujumdar, A. S. (2008). A Review on Nanofluids-Part I: Theoretical and Numerical Investigation. *Brazilian Journal of Chemical Engineering*, 25(4), 613-630. https://doi.org/10.1590/S0104-66322008000400001

[7] Buongiorno, J. (2006). Convective Transport in Nanofluids. *ASME Journal of Heat Transfer*, 128(3), 240-250. https://doi.org/10.1115/1.2150834

[8] Ghalambaz, M., Doostani, A., Izadpanahi, E., & Chamkha, A. J. (2020). Conjugate Natural Convection Flow of Ag–MgO/Water Hybrid Nanofluid in a Square Cavity. *Journal of Thermal Analysis and Calorimetry*, 139(1), 2321-2336. https://doi.org/10.1007/s10973-019-08617-7

[9] Rasool, G., Zhang, T., Chamkha, A. J., Shafiq, A., Tlili, I., & Shahzadi, G. (2020). Entropy Generation and Consequences of Binary Chemical Reaction on MHD Darcy-Forchheimer Williamson Nanofluid Flow Over Non-Linearly Stretching Surface. *Entropy*, 22(1), 18. https://doi.org/10.3390/e22010018

[10] Menni, Y., Chamkha, A. J., Massarotti, N., Ameur, H., Kaid, N., & Bensafi, M. (2020). Hydrodynamic and Thermal Analysis of Water, Ethylene Glycol and Water-Ethylene Glycol as Base Fluids Dispersed by Aluminum Oxide Nano-Sized Solid Particles. *International Journal of Numerical Methods for Heat and Fluid Flow*. https://doi.org/10.1108/hff-10-2019-0739

[11] Bhattacharyya, A., Seth, G. S., Kumar, R., & Chamkha, A. J. (2020). Simulation of Cattaneo-Christov Heat Flux on the Flow of Single and Multi-Walled Carbon Nanotubes Between Two Stretchable Coaxial Rotating Disks.

Journal of Thermal Analysis and Calorimetry, 139(3), 1655-1670. https://doi.org/10.1007/s10973-019-08644-4
[12] Malik, M. Y., Hussain, A., Salahuddin, T., Awais, M., & Bilal, S. (2016). Numerical Solution of Sisko Fluid Over a Stretching Cylinder and Heat Transfer with Variable Thermal Conductivity. *Journal of the Mechanical Behavior of Materials*, 32(1-2), 593-601.
https://doi.org/10.1017/jmech.2016.8
[13] Patel, D. J., Mistri, P. A., & Prajapati, J. J. (2012). Treatment of Cancer by Using Nanoparticles as a Drug Delivery. *International Journal of Drug Development and Research*, 4(1), 14-27.
[14] McCarroll, J., Teo, J., Boyer, C., Goldstein, D., Kavallaris, M., & Phillips, P. A. (2014). Potential Applications of Nanotechnology for the Diagnosis and Treatment of Pancreatic Cancer. *Frontiers in Physiology*, 5, 2.
https://doi.org/10.3389%2Ffphys.2014.00002
[15] Purushotham, S., & Ramanujan, R. V. (2010). Thermoresponsive Magnetic Composite Nanomaterials for Multimodal Cancer Therapy. *Acta Biomaterialia*, 6(2), 502-510. https://doi.org/10.1016/j.actbio.2009.07.004
[16] Abbasi, F. M., Hayat, T., & Ahmad, B. (2015). Peristalsis of Silver-Water Nanofluid in the Presence of Hall and Ohmic Heating Effects: Applications in Drug Delivery. *Journal of Molecular Liquids*, 207, 248-255.
http://dx.doi.org/10.1016%2Fj.molliq.2015.03.042
[17] Kothandapani, M., & Prakash, J. (2015). The Peristaltic Transport of Carreau Nanofluids under Effect of a Magnetic Field in a Tapered Asymmetric Channel: Application of the Cancer Therapy. *Journal of the Mechanical Behavior of Biomedical Materials*, 15(3), 1550030.
https://doi.org/10.1142/S021951941550030X
[18] Hayat, T., & Nadeem, S. (2017). Heat Transfer Enhancement with Ag–CuO/Water Hybrid Nanofluid. *Results in Physics*, 7, 2317-2324.
https://doi.org/10.1016/j.rinp.2017.06.034
[19] Hayat, T., Nadeem, S., Khan, A.U. (2018). Rotating Flow of Ag–CuO/H2O Hybrid Nanofluid with Radiation and Partial Slip Boundary Effects. *The European Physical Journal E*, 41(6), 75. https://doi.org/10.1140/epje/i2018-11682-y
[20] Nadeem, S., Nadeem, A., & Khan, A.U. (2018). Characteristics of Three Dimensional Stagnation Point Flow of Hybrid Nanofluid past a Circular Cylinder. *Results in Physics*, 8, 829-835. https://doi.org/10.1016/j.rinp.2018.01.024
[21] Nadeem, S., Nadeem, A. (2019). On both MHD and Slip Effect in Micropolar Hybrid Nanofluid past a Circular Cylinder under Stagnation Point Region. *Canadian Journal of Physics*, 97(4), 392-399. https://doi.org/10.1139/cjp-2018-0173
[22] Mansour, M.A., Ahmed, S.E., Hady, F.M., Ibrahim, F.S., & Ismaeel, A.M. (2022). Numerical Simulation for Nanofluid Leakage from a Single 2D Blood Vessel. *Alexandria Engineering Journal*, 61(5), 3999-4010.

https://doi.org/10.1016/j.aej.2021.09.029
[23] Bali, R., Prasad, B. (2023). Study of Nanoparticle Diffusion in Capillary-Tissue Exchange System using Jeffrey Nanofluid Model: Effects of Shapes of Nanoparticles. *CFD Letters*, *15*(6), 130–153.
https://doi.org/10.37934/cfdl.15.6.130153
[24] Bali, R., Prasad, B., Mishra, S. (2022). A Review on Mathematical Models for Nanoparticle Delivery In the Blood. 10. 130-146. 10.21474/IJAR01/14526.
http://dx.doi.org/10.21474/IJAR01/14526
[25] Hewlin, R.L., Smith, M., Kizito, J.P. (2023). Computational Assessment of Unsteady Flow Effects on Magnetic Nanoparticle Targeting Efficiency in a Magnetic Stented Carotid Bifurcation Artery. Cardiovasc Eng Tech 14, 694–712.
https://doi.org/10.1007/s13239-023-00681-3
[26] Hewlin, R.L., Jr.; Tindall, J.M. (2023). Computational Assessment of Magnetic Nanoparticle Targeting Efficiency in a Simplified Circle of Willis Arterial Model. Int. J. Mol. Sci 24, 2545.
https://doi.org/10.3390/ijms24032545
[27] Stanley, N., Ciero, A., Timms, W., and Hewlin, R. L., Jr. (2023). A 3-D Printed Optically Clear Rigid Diseased Carotid Bifurcation Arterial Mock Vessel Model for Particle Image Velocimetry Analysis in Pulsatile Flow ASME Open J. Engineering ASME. January 2 021010.
https://doi.org/10.1115/1.4056639
[28] Ismaeel, A.M., Mansour, M.A., Ibrahim, F., Hady, F.M. (2022). Numerical Simulation for Nanofluid Extravasation from a Vertical Segment of a Cylindrical Vessel into the Surrounding Tissue at the Microscale. *Applied Mathematics and Computation*, 417, 126758. https://doi.org/10.1016/j.amc.2021.126758
[29] Ismaeel, A.M., Kamel, R.S., Hedar, M.R., & Hady, F.M. (2023). Numerical Simulation for a Casson Nanofluid over an Inclined Vessel Surrounded by Hot Tissue at the Microscale. *SN Applied Sciences*, 5(8), 223.
https://doi.org/10.1007/s42452-023-05436-2
[30] Kamel, R.S., Ismaeel, A.M., & Hady, F.M. (2023). Numerical Study for a Newtonian Nanofluid over a Vertical Cylindrical Vessel Surrounded by a Hot Tissue. *SN Applied Sciences*, 5, 315.
https://doi.org/10.1007/s42452-023-05527-0
[31] Shafey, A. M. E., Alharbi, F. M., Javed, A., Abbas, N., ALrafai, H. A., Nadeem, S., Issakhov, A. (2021). Theoretical analysis of Brownian and thermophoresis motion effects for Newtonian fluid flow over nonlinear stretching cylinder. *Case Studies in Thermal Engineering*, 28, 101369.
https://doi.org/10.1016/j.csite.2021.101369
[32] Ismaeel AM (2020). A mathematical model for photothermal therapy of spherical tumors. PhD thesis, University of Glasgow.
https://doi.org/10.5525/gla.thesis.80268

Nomenclature

C nanoparticle concentration.
C_w nanoparticle concentration at the upper wall.
C_p Specific heat at constant pressure.
C_∞ Concentration in ambient flow.
T_∞ Ambient fluid temperature.
D_T Thermophoresis coefficient.
D_B Brownian motion coefficient.
N_b Brownian motion parameter.
N_t Thermophoresis parameter.
p Fluid pressure.
P Dimensionless pressure.
P_r Prandtl number.
Nu_z Nusselt number.
R_e Reynolds number.
B_0 magnetic field strength.
T temperature
SAR The specific absorption rate.
S_c Schmidt number.
Q Heat generation/absorption parameter
Q_H heat flux into the blood vessel.
u, w Velocity components in r, z directions.
U, W Dimensionless velocity components.

Greek symbols

α Thermal diffusivity.
ϕ dimensionless nanoparticle concentration.
σ Effective electrical conductivity.
σ^* Stefan-Boltzmann constant.
θ Dimensionless temperature.
μ Dynamic viscosity.
ν Kinematic viscosity.
ρ Density.
λ heat source coefficient.
γ dimensionless constant velocity.
a Radius of cylinder.
M_0 magnetic field parameter.

Subscripts

0 Reference.
f Pure fluid.
e_{ff} effective.
w wall.

Figures

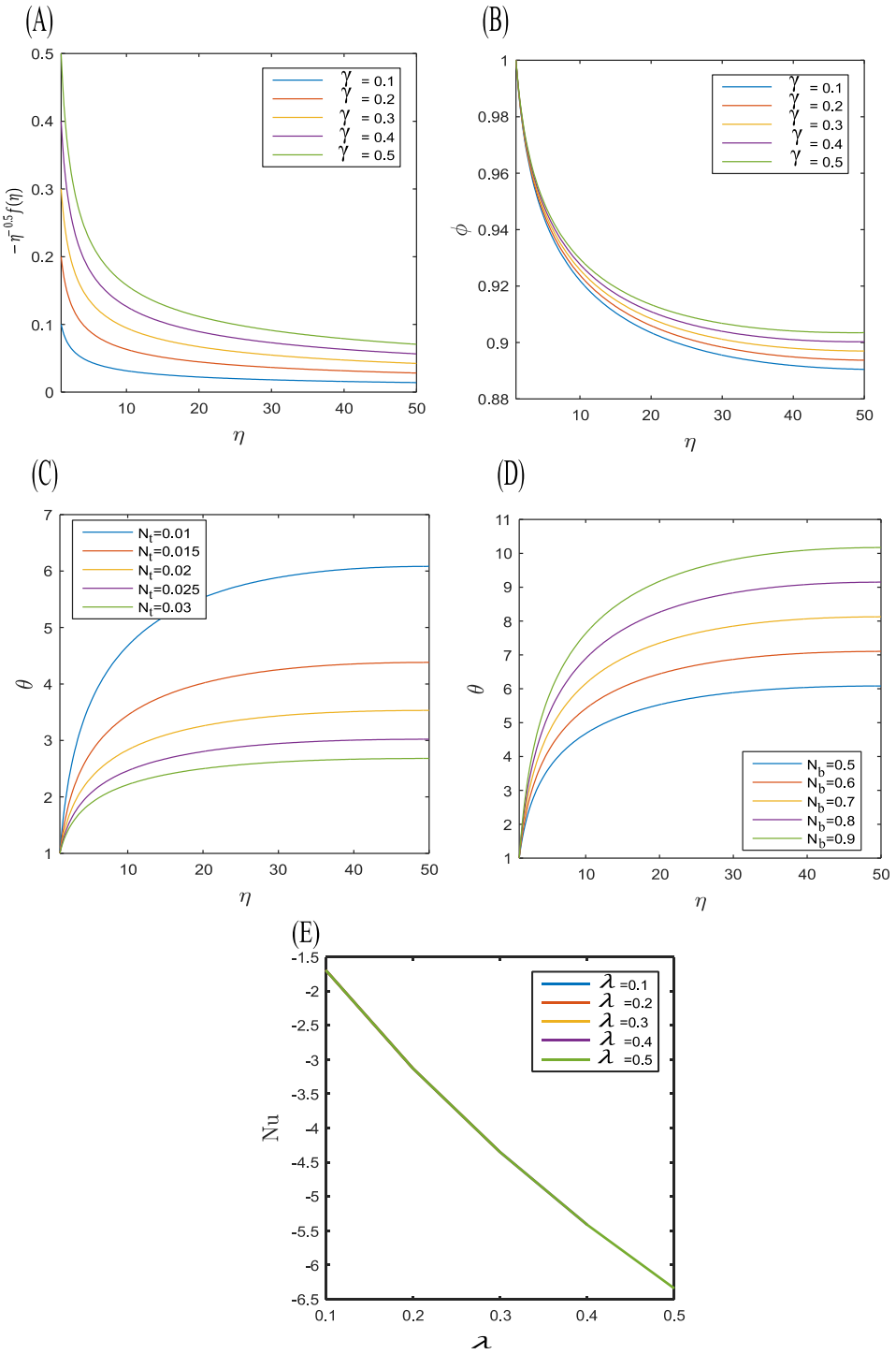

Figures 2: (A) The interstitial nanofluid radial velocity for different values of γ. (B) NP concentration for different values of γ. (C) Nanofluid temperature for different values of N_t. (D) Nanofluid temperature for different values of N_b. (E) the Nusselt number for different values of λ.

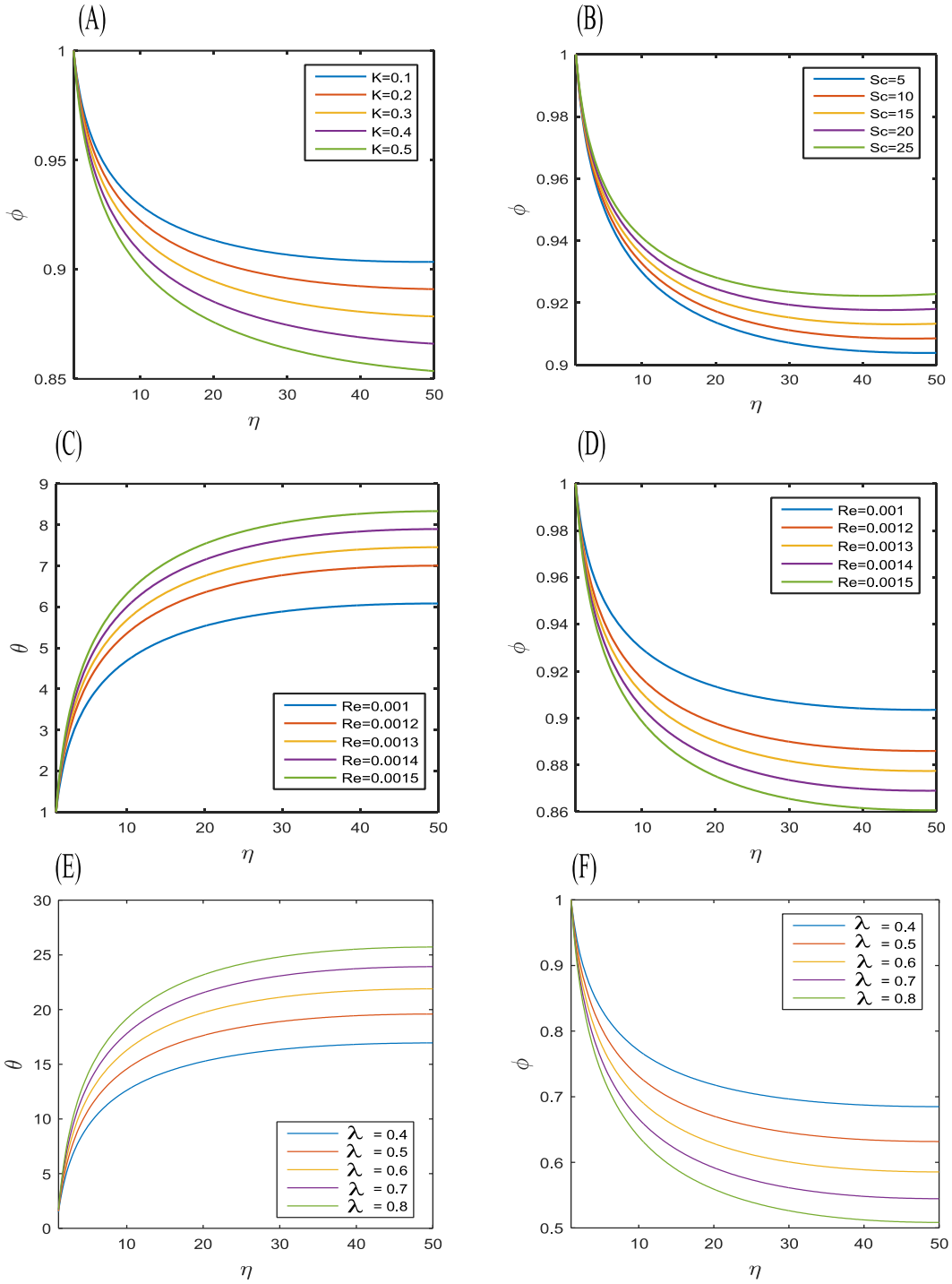

Figures 3: Numerical results of nanofluid temperature and NP concentration: (A) NP concentration for different values of K. (B) NP concentration for different values of Sc. (C) Nanofluid temperature for different values of Re. (D) NP concentration for different values of Re. (E) Nanofluid temperature for different values of λ. (F) NP concentration for different values of λ.